ACS APPLIED MATERIALS & INTERFACES

Research Article

www.acsami.org

Fabrication of Functional Nanowire Devices on Unconventional Substrates Using Strain-Release Assembly

John W. Durham, III and Yong Zhu*

Department of Mechanical and Aerospace Engineering, North Carolina State University, Raleigh, North Carolina 27695-7910, United States

Supporting Information

ABSTRACT: We report three representative nanowire (NW) devices for applications in stretchable electronics, strain sensing, and optical sensing. Fabrication of such devices is based on a recently developed strain-release assembly method. NWs are first aligned transversely on an elastomeric substrate using the strain-release assembly. Constant resistance is achieved in silicon (Si) NW devices stretched up to ~40% of axial strain, highlighting a new concept of transverse buckling. Combining the NW assembly with transfer printing extends suitable device substrates beyond elastomers to other unconventional materials (e.g., flexible and transparent materials). Following this combined process, flexible SiNW strain sensors are fabricated on plastics capable of sensing up to 1.6% bending strain and gauge factors >1000; flexible zinc oxide NW ultraviolet sensors are demonstrated with quick recovery (~2 s) and excellent repeatability on plastics. Our results show promise for the strain-release assembly as a simple and cost-effective process to fabricate NW devices on unconventional substrates.

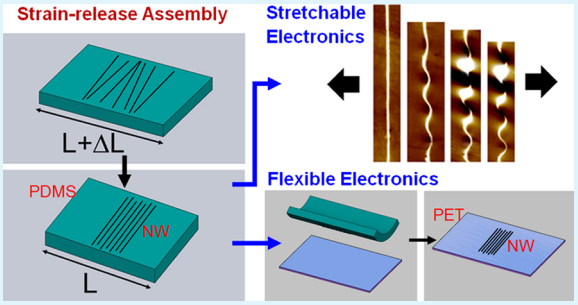

KEYWORDS: *nanowire, assembly, transfer printing, flexible electronics, strain sensor, UV sensor, stretchable electronics*

1. INTRODUCTION

Many applications with nanowires (NWs) as active materials in electronic devices and sensors have been developed.[1,2] Unconventional electronics such as flexible and stretchable electronics enables novel device applications whose versatility exceeds that of the planar, rigid counterparts. Recently, semiconductor NWs have shown promising potential for the applications of flexible and stretchable electronics,[3−10] where assembly of NWs on flexible and stretchable substrates represents a key step. The processing limitations of these unconventional substrate materials, elastomers in particular, make such device fabrication more challenging compared to conventional hard substrates.[11] The ability to effectively align, assemble and transfer NWs on flexible and stretchable substrates is thus of great importance. A number of methods have been developed for the assembly and alignment of NWs such as flow-assisted alignment, Langmuir-Blodgett technique, external field-assisted alignment and contact printing; interested readers are referred to recent reviews[4,6] Though some of these methods are compatible with flexible substrates (e.g., plastics), almost none are with stretchable substrates (e.g., elastomers).

An alternative method, strain-release assembly, was recently developed for aligning semiconductor and metal NWs on elastomeric substrates (e.g., polydimethylsiloxane, PDMS).[12] This method offers a simple and effective approach to achieve highly aligned NWs with large area coverage and controlled density; the NWs could be from either as-grown substrates (e.g., Si NWs) or solution-based dispersions (e.g., Ag NWs).

In the present work, we demonstrated the utility of the strain-release assembly in fabricating functional NW devices on different unconventional substrates (e.g., stretchable and flexible substrates). A modified transfer printing process[13−16] was developed which uses the alignment substrate (i.e., PDMS) itself as the "stamp" to transfer aligned NWs to other types of substrates. Three representative devices were fabricated and characterized to show applications in stretchable electronics, strain sensing and optical sensing. Integrating the strain-release method for NW alignment/assembly with the transfer printing to diverse substrates provides a simple and scalable approach for developing NW-based unconventional devices.

2. RESULTS AND DISCUSSION

The as-grown NWs were transferred by contact printing[17] onto a pre-strained PDMS substrate (90% pre-strain), which was then released to align the NWs in the transverse direction (Figure 1a-d).[12] The NWs are uniformly aligned across millimeter length scales with relatively high densities (2−3 NW/μm). These aligned NWs form the basis for subsequent device developments.

2.1. Stretchable, Constant-Resistance Devices. Buckling is a commony used strategy in stretchable electronics.[5,18] Typically NWs are aligned in the axial direction in an axially pre-strained substrate; upon release of the pre-strain, the NWs

Received: July 5, 2012
Accepted: December 18, 2012
Published: December 18, 2012

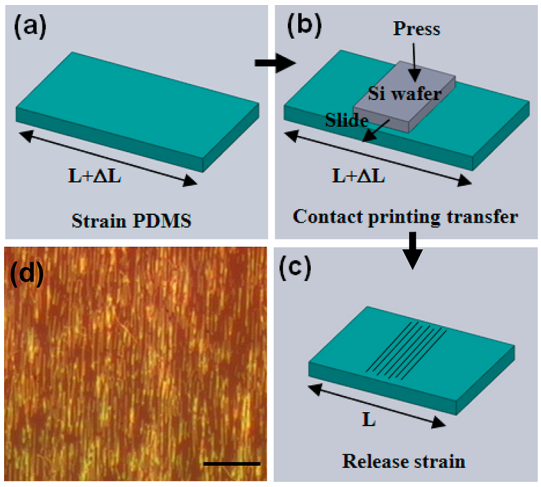

Figure 1. (a–c) Schematic of the strain–release assembly method and (d) optical image of resulting SiNWs aligned in the transverse direction on PDMS (scale bar 10 μm).

are buckled and become stretchable up to the pre-strain. Following this approach, we fabricated stretchable electronic devices by buckling the aligned NWs on prestrained PDMS substrate.[5] Two buckling modes (i.e., 2D wave versus 3D coil) were obtained in a controlled fashion by tuning ultraviolet (UV)/ozone treatment of the PDMS surface.[5,19]

However, the stretchable NW device presented in this work operates on a new concept of transverse buckling. In these devices, the NWs are transversely aligned. Under tensile strain in the axial direction, transverse NWs undergo compressive strain, but at much reduced level compared to the axial strain via the Poisson's effect. The compressive strain might result in buckling of the transversely aligned NWs. Figure 2a shows an atomic force microscopy (AFM) image of a buckled NW, where the 3D coiled shape can be seen.[5]

A layer of nickel (400 nm thick, Ohmic contact) was deposited using electron beam evaporation through a shadow mask onto the NWs to serve as electrodes (inset of Figure 2b). Each device consists of two electrodes in the transverse direction (25 by 25 μm) and NWs in between (10 μm gap). The geometry of the deposited electrode pads effects the strain distribution across the PDMS surface due to "island in the sea"

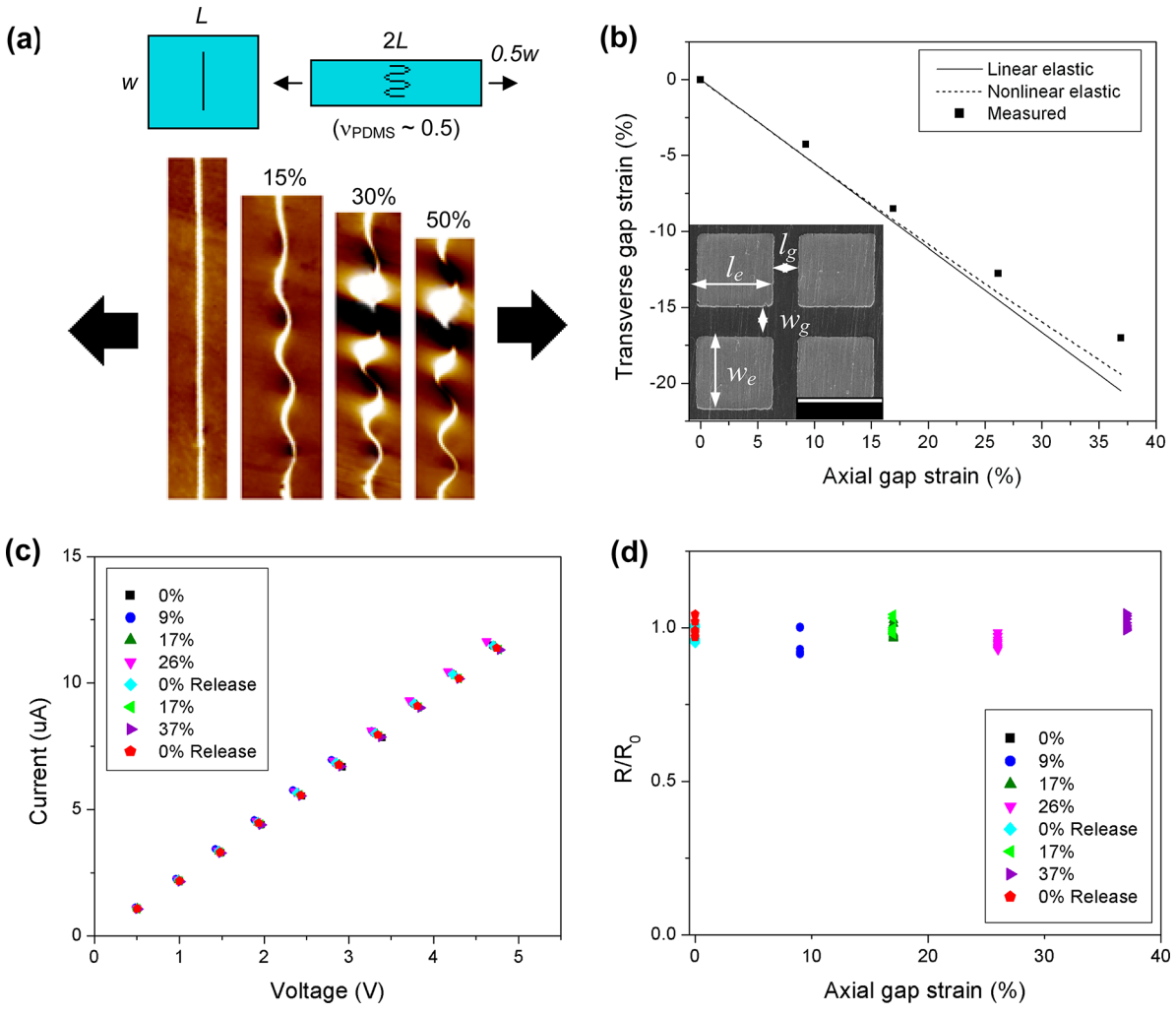

Figure 2. (a) Top, schematic showing NW buckling in the transverse direction due to Poisson effect on PDMS. Bottom, AFM images of NW buckling under various strains applied in the axial direction. (b) Linear elastic and nonlinear elastic model comparison with measured gap strain values. Inset is SEM image of SiNW array devices on PDMS after deposition of Ni electrodes and device parameters (scale bar 25 μm). (c) I–V characteristics under loading/unloading and (d) resistance change under loading/unloading showing constant performance to large strains.

dx.doi.org/10.1021/am302384z | ACS Appl. Mater. Interfaces 2013, 5, 256–261

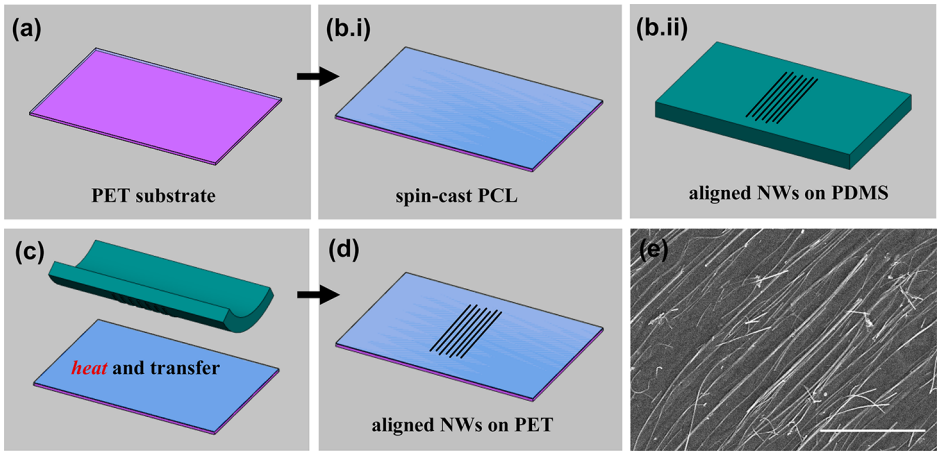

Figure 3. (a–b.i) NW transfer printing schematic including adhesion layer deposition, (b.ii) NW assembly on PDMS stamp, and (c, d) heated contact transfer printing to PET. (e) SEM image of aligned SiNWs after transfer to PET (scale bar 5 μm).

mechanics (i.e., the electrodes are much stiffer than the PDMS and thus undeformed).[20] Assuming a linear elastic approximation of PDMS, the axial and transverse gap strains due to the overall applied strain, ε_{app} is shown to be

$$\varepsilon_{axial} = \varepsilon_{app}\left(\frac{l_g + l_e}{l_g}\right) \quad (1)$$

$$\varepsilon_{trans} = -\nu\varepsilon_{app}\left(\frac{w_g + w_e}{w_g}\right) \quad (2)$$

where ν is Poisson's ratio of PDMS, l_g and w_g are the respective gap distances of the PDMS between electrodes in the axial and transverse directions, and l_e and w_e are the length and width of the electrodes, respectively. A more accurate, nonlinear elastic model of PDMS leads to the axial and transverse gap strains, viz.

$$\varepsilon_{axial} = \varepsilon_{app}\left(\frac{l_g + l_e}{l_g}\right) \quad (3)$$

$$\varepsilon_{trans} = ((\varepsilon_{app} + 1)^{-0.5} - 1)\left(\frac{w_g + w_e}{w_g}\right) \quad (4)$$

Both models assume that the electrodes are sufficiently rigid to constrain the applied strain to the PDMS gap between them.

Measurement of the gap distances and electrode geometries under applied strain via in situ optical microscopy imaging were compared with the theoretical strain models (Figure 2b). Both models were found to agree reasonably well with the experimental results; the nonlinear model agreed better for large strain. The difference observed between models and experiments might arise from the image analysis and the existence of some small strains in the electrodes. Cyclic loading was applied to the PDMS substrate (in the direction orthgonal to the NWs) by the Fullam mechanical testing stage loaded in a probe station (Micromanipulator). The current–voltage (I–V) response of the Si NW devices was measured simultaneously using tungsten probe tips. Figure 2c shows the I–V response as a function of the applied strain. Axial gap strain is used to describe the applied strains because the geometry of the gap with respect to that of the electrode is a factor that can be adjusted to improve overall applied strain without influencing the capabilities of the device materials. The gap strains (axial and transverse) are thus the important parameters in this experiment and serve to evaluate the effectiveness of this method. There was negligible change in the I–V characteristics for strains up to ~40% (Figure 2d). Small decreases in the device resistance probably stems from improvement in the NW-metal contact with applied compressive strains in the transverse direction. The device showed excellent stability under repeated loading and unloading cycles.

The advantages of the transverse buckling is twofold: (1) the compressive strain in NWs is much smaller due to the Poisson's effect for the same axial stretching range that the devices undergo, and (2) there is no need of pre-straining the PDMS substrate.[5] The new device configuration is favorable for uniaxial stretching, though it might be modest for biaxial stretching—the maximum tension in the transverse direction is up to the fracture strain of the NWs that is size-dependent (over 12% for Si NWs of 15 nm in diameter[21]). Constant electric performance under large strains is critical for many applications such as stretchable transistors, diodes, sensors and solar cells.

2.2. Flexible Strain Sensors. PDMS has been employed as a stamping material by which to transfer materials even devices, from a rigid, planar substrate to unconventional substrates such as plastic or glass.[6,13,14] Since our strain-release assembly method utilizes PDMS to induce the alignment of NWs, it could be seamlessly integrated into a similar transfer printing process. This would enable the use of other materials as the final substrate, greatly expanding the versatility of the strain-release assembly method for device fabrication. To demonstrate the feasibility of using the alignment process in conjunction with the PDMS stamping, we have fabricated NW devices on a flexible plastic—polyethylene terephthalate (PET)—substrate.

The PET substrate was coated with a thin layer of polycaprolactone (PCL) by spin-coating a PCL-toluene solution on the PET surface (Figure 3a, b.i). The PCL served as an adhesion layer to promote the transfer of NWs from the PDMS to the plastic.[22] SiNWs were aligned separately on PDMS via the strain-release method with 90% pre-strain as described above (Figure 3b.ii). The NWs were then transferred to the PET by a heated contact printing process (Figure 3c, d). Approximately 85% of the NWs were transferred to the plastic substrate by this process after transfer to the PET, as seen in

Figure 3e. Titanium electrodes, forming Schottky-contact with Si,[23] were deposited using the same process above to fabricate SiNW array devices on PET; the NWs were aligned in the longitudinal direction with respect to the applied load. The same shadow mask was used, so the same device size (25 μm by 25 μm electrodes and 10 μm wide gap) was obtained. The electrical performance (i.e., $I-V$ characteristic) of a device under bending was measured as the two clamped ends of the substrate were brought closer together by the Fullam mechanical testing stage in the probe station (Figure 4a).

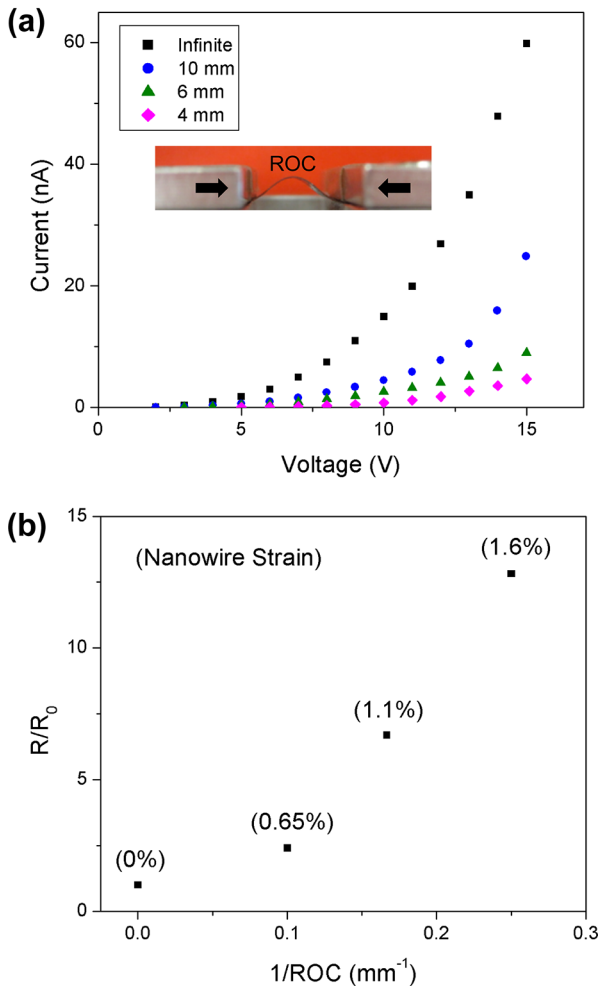

Figure 4. (a) $I-V$ performance of SiNW device on PET under bending. Inset image is of custom mechanical stage used during bending experiments with radius of curvature (ROC) location indicated. ROC values are given in the ligand. (b) Resistance change and NW tensile strain with respect to ROC.

The device was able to bend to a small radius (4 mm). The resistance increased with increasing curvature and the strain in the NW can be calculated from the radius of curvature using classic beam bending mechanics (Figure 4b). The maximum strain in the NW was ~1.6%, well below the fracture strain of the 20–50 nm diameter SiNWs as previously reported by our group,[21] indicating a reliable device able to bend to small radii without failure. The sensitivity of the device was measured by the gauge factor GF,

$$GF = \frac{\Delta R}{R}\varepsilon^{-1} \quad (5)$$

where R is the resistance, and ε is the mechanical strain. Our strain sensor device exhibited very large gauge factors (from 300 to >1000) depending on the strain level, which far exceeds that of conventional metal strain gauges and compares well with other NW-based strain sensors.[14,24,25]

2.3. Flexible UV Sensors. Zinc oxide (ZnO) NW UV sensors were fabricated similarly on plastic by the strain-release assembly method in conjunction with the PDMS transfer printing process to a PCL-coated PET substrate. The ZnO NWs were also aligned with 90% PDMS pre-strain. Titanium electrodes, forming ohmic contacts with ZnO,[26,27] were deposited to fabricate two-terminal ZnO NW devices on flexible plastic. Under UV exposure (BHK Analamp Mercury lamp, ~30 μW cm^{-2} for 365 nm at a distance of 20 cm from the lamp), the resistances of the ZnO NWs decreased significantly, allowing for sensitive detection of light in the UV range. The dark $I-V$ characteristics along with UV illumination response for one such single-NW device are shown in Figure 5a. This response is due to the presence of adsorbed oxygen molecules on the NW surfaces, which are desorbed by recombination with holes on the surface after photo-induced electron-hole pair generation inside the NW.[28,29] The unpaired electrons left behind directly lead to a measurable increase in current under an applied bias.

Cycling the UV lamp on and off resulted in repeatable sensor response and recovery from the NW device (Figure 5b). On–off cycles were performed at a 1:2 time ratio to allow for sufficient device recovery between cycles. UV photocurrent response on-off ratios ranged from approximately 3.5:1 to 15:1 for our devices, lower than that of other reported ohmic devices (>100),[28−32] which might be due to a low-intensity UV source and/or small NW diameter used in our devices (20–80 nm compared to 200 nm and 150–300 nm as previously reported[28,32]). The recovery time of the sensor, defined as the time for current to decrease to 1/e (37%) of the on-current after the lamp has been switched off, was found to be as fast as ~2.3 s (Figure 5c). This recovery time is quicker than similar ohmic contact ZnO NW UV sensors previously reported,[28] which can also be attributed to the smaller NW diameters used in our devices. It was shown that smaller ZnO NW diameters exhibited faster recovery times.[28] Comparing our ZnO NW UV sensor with other similar UV sensors indicates a benefit of our device in its fast recovery, making it suitable for fast sensing operation where very large photocurrent gain is not required. Our sensors demonstrated potential for optical sensing and switching device applications on flexible substrates.

3. CONCLUSIONS

In summary, we have demonstrated the fabrication of three types of NW devices using the strain-release assembly method that enables transference to unconventional substrates when combined with transfer printing. The devices address a range of potential applications: (1) a stretchable SiNW device that is built on the new concept of transverse buckling exhibits constant performance across a large strain range with applications in stretchable electronics; (2) a flexible SiNW strain sensor shows very large gauge factor; (3) a flexible ZnO NW UV sensor shows reliable photo-response and fast recovery for optoelectronic sensing and switching applications. The demonstrated fabrication process can be readily applied to other one-dimensional nanostructures such as carbon nanotubes.[33−35] The results herein exemplify the versatility of our assembly process through realization of various functional

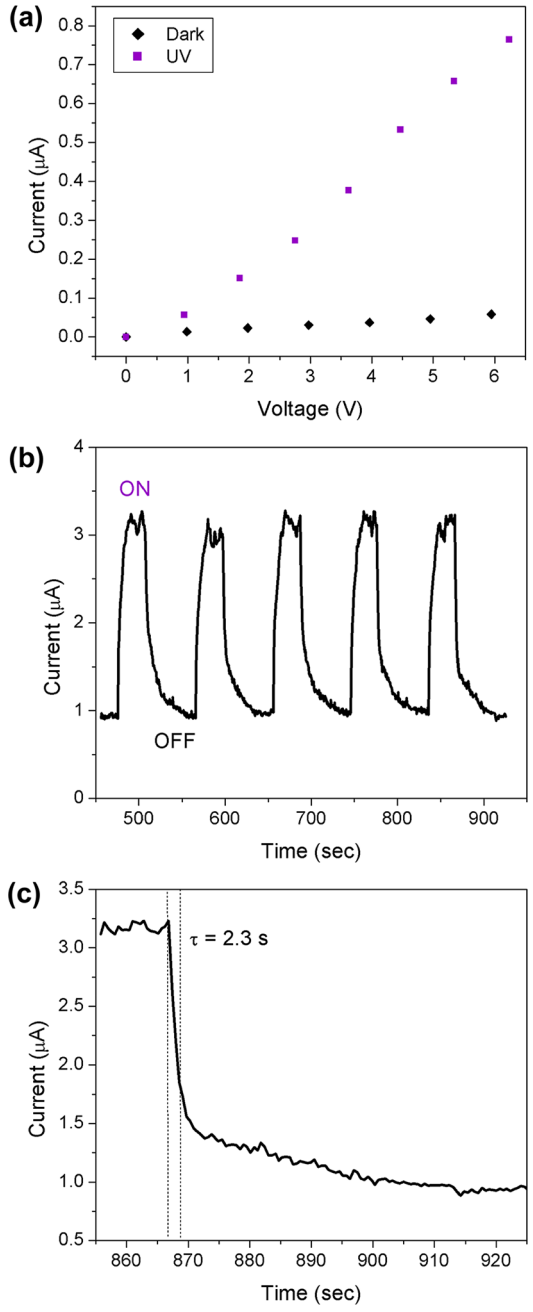

Figure 5. (a) Dark (off) vs. photoresponse (on) *I*–*V* measurements of ZnO NW UV sensor. (b) Sensor photocurrent response to cyclic UV illumination in air at a bias of 20 V. (c) Recovery response of the NW sensor.

device types on unconventional substrates in a simple, scalable, and effective manner.

EXPERIMENTAL SECTION

Both Si and ZnO NWs were synthesized by the vapor-liquid-solid (VLS) method on Si/SiO2 substrates with Au colloids as the catalysts.[21,36,37] The NW diameters are determined by the size of the Au colloids; the diameters for Si and ZnO NWs are 15–60 nm and 20–80 nm, respectively. The NW lengths typically range from 5 to 30 μm. Both Si and ZnO NWs in this study are single crystalline. Si NWs grow primarily along ⟨111⟩ (though ⟨110⟩ and ⟨112⟩ directions are possible for NWs with smaller diameter); ZnO NWs grow along ⟨0001⟩ direction. Si NWs have little or no visible amorphous oxide layer on the NW surface. More details on the NW synthesis and structural characterization can be seen in the Supporting Information.

PDMS was prepared at 10:1 ratio of Dow Corning SYLGARD 184 elastomer and curing agent, respectively. UVO treatment of the PDMS surface was performed for 5 minutes for stretchable device fabrication. Device stretching was achieved by a custom-built mechanical testing stage and directly observed under optical microscopy while probing via micromanipulator stage for in situ *I*–*V* measurements.

PCL pellets were dissolved in a toluene solution and heated to 65 °C while stirring for 60 min to ensure a uniform solution. PET was rinsed in acetone and DI water before PCL deposition was performed via dynamic spin-coating at 1000 rpm for a duration of 60 s to form a thin adhesion layer (10-30 nm thick).[22] To transfer the NWs, we pre-heated PCL-coated PET and PDMS to the melting point of PCL (~65 °C), placed them in contact for 5 min, and then peeled off the PDMS to complete the process. PET bending was performed by applying compressive strain with the mechanical testing stage to induce bending. Radius of curvature was measured at the device position (chosen such that the device experienced the largest curvature under bending).

ASSOCIATED CONTENT

Supporting Information

This material is available free of charge via the Internet at http://pubs.acs.org.

AUTHOR INFORMATION

Corresponding Author

*E-mail: yong_zhu@ncsu.edu.

Notes

The authors declare no competing financial interest.

ACKNOWLEDGMENTS

This work was supported by the North Carolina Space Grant and the National Science Foundation under Awards CMMI-1129817 and EEC-1160483 (Nanosystems Engineering Research Center). We thank W. Lu at the University of Michigan and Y. Gu at Washington State University for providing Si and ZnO NWs, respectively.

REFERENCES

(1) Lu, W.; Lieber, C. M. *J. Phys. D.: Appl. Phys.* **2006**, *39*, R387–R406.
(2) Xia, Y.; Yang, P.; Sun, Y.; Wu, Y.; Mayers, B.; Gates, B.; Yin, Y.; Kim, F.; Yan, H. *Adv. Mater.* **2003**, *15*, 353–389.
(3) McAlpine, M. C.; Ahmad, H.; Wang, D.; Heath, J. R. *Nat. Mater.* **2007**, *6*, 379–384.
(4) Fan, Z.; Ho, J. C.; Takahashi, T.; Yerushalmi, R.; Takei, K.; Ford, A. C.; Chueh, Y.-L.; Javey, A. *Adv. Mater.* **2009**, *21*, 3730–3743.
(5) Xu, F.; Lu, W.; Zhu, Y. *ACS Nano* **2010**, *5*, 672–678.
(6) Liu, X.; Long, Y.-Z.; Liao, L.; Duan, X.; Fan, Z. *ACS Nano* **2012**, *6*, 1888–1900.
(7) Duan, X. *MRS Bull.* **2007**, *32*, 134–141.
(8) Takei, K.; Takahashi, T.; Ho, J. C.; Ko, H.; Gillies, A. G.; Leu, P. W.; Fearing, R. S.; Javey, A. *Nat. Mater.* **2010**, *9*, 821–826.
(9) Javey, A.; Nam; Friedman, R. S.; Yan, H.; Lieber, C. M. *Nano Lett.* **2007**, *7*, 773–777.
(10) Ryu, S. Y.; Xiao, J.; Park, W. I.; Son, K. S.; Huang, Y. Y.; Paik, U.; Rogers, J. A. *Nano Lett.* **2009**, *9*, 3214–3219.
(11) Lee, J.; Park, C.; Whitesides, G. *Anal. Chem.* **2003**, *75*, 6544–6554.
(12) Xu, F.; Durham, J. W.; Wiley, B. J.; Zhu, Y. *ACS Nano* **2011**, *5*, 1556–1563.
(13) Sun, Y.; Rogers, J. A. *Nano Lett.* **2004**, *4*, 1953–1959.
(14) Lee, C. H.; Kim, D. R.; Zheng, X. *Proc. Natl. Acad. Sci. U.S.A.* **2010**, *107*, 9950–9955.

(15) Hsieh, G.-W.; Wang, J.; Ogata, K.; Robertson, J.; Hofmann, S.; Milne, W. I. *J. Phys. Chem. C* **2012**, *116*, 7118−7125.
(16) Madaria, A.; Kumar, A.; Ishikawa, F.; Zhou, C. *Nano Res.* **2010**, *3*, 564−573.
(17) Fan, Z.; Ho, J. C.; Jacobson, Z. A.; Yerushalmi, R.; Alley, R. L.; Razavi, H.; Javey, A. *Nano Lett.* **2008**, *8*, 20−25.
(18) Rogers, J. A.; Someya, T.; Huang, Y. *Science* **2010**, *327*, 1603−1607.
(19) Qin, Q.; Zhu, Y. *ACS Nano* **2011**, *5*, 7404−7410.
(20) Lacour, S.; Jones, J.; Wagner, S.; Li, T.; Suo, Z. *Proc. IEEE* **2005**, *93*, 1459−1467.
(21) Zhu, Y.; Xu, F.; Qin, Q.; Fung, W. Y.; Lu, W. *Nano Lett.* **2009**, *9*, 3934−3939.
(22) Hyun, D. C.; Moon, G. D.; Cho, E. C.; Jeong, U. *Adv. Funct. Mater.* **2009**, *19*, 2155−2162.
(23) Motayed, A.; Bonevich, J. E.; Krylyuk, S.; Davydov, A. V.; Aluri, G.; Rao, M. V. *Nanotechnology* **2011**, *22*, 075206.
(24) He, R.; Yang, P. *Nat. Nanotechnol.* **2006**, *1*, 42−46.
(25) Zhou, J.; Gu, Y.; Fei, P.; Mai, W.; Gao, Y.; Yang, R.; Bao, G.; Wang, Z. L. *Nano Lett.* **2008**, *8*, 3035−3040.
(26) Kim, S.; Jang, H.; Kim, J.; Jeon, C.; Park, W.; Yi, G.; Lee, J. *J. Electron. Mater.* **2002**, *31*, 868−871.
(27) Chang, P.-C.; Fan, Z.; Chien, C.-J.; Stichtenoth, D.; Ronning, C.; Lu, J. G. *Appl. Phys. Lett.* **2006**, *89*, 133113.
(28) Soci, C.; Zhang, A.; Xiang, B.; Dayeh, S. A.; Aplin, D. P. R.; Park, J.; Bao, X. Y.; Lo, Y. H.; Wang, D. *Nano Lett.* **2007**, *7*, 1003−1009.
(29) Liu, B.; Wang, Z.; Dong, Y.; Zhu, Y.; Gong, Y.; Ran, S.; Liu, Z.; Xu, J.; Xie, Z.; Chen, D.; Shen, G. *J. Mater Chem.* **2012**, *22*, 9379−9384.
(30) Kind, H.; Yan, H.; Messer, B.; Law, M.; Yang, P. *Adv. Mater.* **2002**, *14*, 158−160.
(31) Wu, W.; Bai, S.; Cui, N.; Ma, F.; Wei, Z.; Qin, Y.; Xie, E. *Sci. Adv. Mater.* **2010**, *2*, 402−406.
(32) Yang, Q.; Guo, X.; Wang, W.; Zhang, Y.; Xu, S.; Lien, D. H.; Wang, Z. L. *ACS Nano* **2010**, *4*, 6285−6291.
(33) Engel, M.; Small, J. P.; Steiner, M.; Freitag, M.; Green, A. A.; Hersam, M. C.; Avouris, P. *ACS Nano* **2008**, *2*, 2445−2452.
(34) Zhu, Y.; Xu, F. *Adv. Mater.* **2012**, *24*, 1073−1077.
(35) Xu, F.; Wang, X.; Zhu, Y. T.; Zhu, Y. *Adv. Funct. Mat.* **2012**, *22*, 1279−1283.
(36) Xu, F.; Qin, Q.; Mishra, A.; Gu, Y.; Zhu, Y. *Nano Res.* **2010**, *3*, 271−280.
(37) Soudi, A.; Khan, E. H.; Dickinson, J. T.; Gu, Y. *Nano Lett.* **2009**, *9*, 1844−1849.